RAPID COMMUNICATIONS

PHYSICAL REVIEW E VOLUME 52, NUMBER 2 AUGUST 1995

Flow topology associated with disjoint eddies in an asymmetric film-splitting problem

P.J. Wicks, M. Decré, Ph. Planquart, and J.M. Buchlin
von Karman Institute for Fluid Dynamics, Ch. de Waterloo, 72, B-1640 Rhode-Saint-Genèse, Belgium
(Received 9 February 1995)

In a film-splitting problem where recirculation is present, theoretical arguments lead to the *joint eddy* flow topology, where two eddies, attached to the interface, share a common streamline, and the *disjoint eddy* topology, where only one eddy attaches to the interface. The second, interior eddy is then separated from the former by a meandering streamtube. The disjoint eddy topology is shown to be generic if any asymmetry source is present. Original measurements of the velocity vector field are combined with spectral element simulations of the flow to support the theoretical developments.

PACS number(s): 47.15.Gf, 47.11.+j, 68.10.−m

The film-splitting flow considered in this paper may be thought of as a type of Hele-Shaw cell with slowly diverging walls. It constitutes the stable state of directional viscous fingering (DVF), a one-dimensional system which has recently been studied quite extensively [1]. The flow occurs in an industrial process known as *roll coating* in which two moving cylinders drag a fluid through a very thin gap, where it splits into two films, one attached to each cylinder. An adverse pressure gradient keeps the fluid-air interface stationary in the laboratory frame of reference. An instability called *ribbing*, analogous to DVF, occurs when the cylinder velocities exceed a critical value; it is the subject of many investigations [2]. The features of the flow under consideration—a highly curved interface near slowly diverging walls at low velocities—are also seen in other situations such as flows near a sharp corner or interface shapes near dipoles [3]. Understanding of the flow topology is thus of quite general interest. The symmetry of the problem about a plane [shown as a dotted line in Fig. 1(c)] going through the center of the gap, and parallel to the cylinder axes and to the flow direction, may be broken in three ways. First, there may be a component of gravity acting across the flow. Second, the cylinders may have different radii. Third, they may have different velocities.

There is considerable analytical [4] and numerical [5,6] work on this flow. Three types of flow topology have come to be associated with the region of flow downstream of the thinnest part of the gap (the "nip"), in cases where the flow is steady and the flow rate is sufficient for the flow through the nip to be unidirectional. The simplest is shown in Fig. 1(a). The flow divides at the stagnation point on the free surface, one part of the flow forming the upper film, the other forming the lower film. This topology is known to occur when the cylinder velocities are relatively high [4–7]. It has long been known that at lower speeds a recirculating flow topology forms, in which there are six stagnation points: three on the meniscus, one interior separation point, and two eddy centers. This recirculation has generally been assumed to have the *joint* eddy structure shown in Fig. 1(b) [4]. However, asymmetric finite element solutions reveal an asymmetric flow structure, shown in Fig. 1(c) [5]. In this case the eddies are *disjoint*, one of them being detached from the free surface and allowing a wedge of fluid to move around it and "snake" back between the two eddies, finally attaching itself to the opposite cylinder. Which topology will be encountered in practice is a major question for roll coating, since the presence of the "snake" will modify the mass transfer between the cylinders.

On the experimental side, work has until recently been mainly restricted to the measurement of the applied film thicknesses downstream of the film-splitting zone [4,5]. The evolution of experimental techniques in this field [7–9] has led to quantitative knowledge of the film-splitting shape [10] and detailed measurement of the velocity field beneath the free surface.

In the following, we provide full evidence that for stable asymmetric film-splitting problems where recirculation is present, the flow topology is of the *disjoint eddy* type: first, on the basis of theoretical considerations using dynamical systems theory, second, by performing original particle image displacement velocimetry (PIDV) measurements in the vicinity of the free surface, and finally by comparing these results with a spectral element simulation for the corresponding Navier-Stokes problem. For a review of PIDV, see [11].

The purpose of the theoretical analysis is to apply simple dynamical systems theory to demonstrate that the asymmetric flow topology of Fig. 1(c) is more generic than the symmetric one, and will therefore always be seen in practice unless the operating conditions are entirely symmetric. Symmetric operating conditions imply equal roller speeds and radii, and gravity acting along the line of symmetry of the flow.

Two arguments are proposed. The first argument concerns the structure of the separation streamlines linking the stagnation points and their stability to a small symmetry-breaking

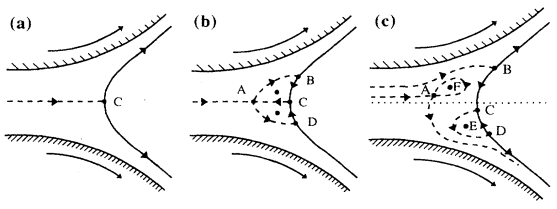

FIG. 1. Possible 2D flow topologies for a film-splitting problem. Dashed lines represent inner streamlines, the full line displays the fluid-air interface. (a) no eddies; (b) symmetric, joint eddies; (c) asymmetric, disjoint eddies.

perturbation. The second argument concerns the nature of the transition from nonrecirculating to recirculating flow, as a parameter such as the mean roller speed is varied.

First, the symmetric flow of Fig. 1(b) contains two sets of streamlines, $ABCA$ and $ADCA$, that are heteroclinic orbits, each linking three stagnation points. In contrast, Fig. 1(c) contains only one pair of heteroclinic orbits, DCD, and one homoclinic orbit AA. We consider the effect of a small symmetry-breaking perturbation of the flow of Fig. 1(b) in which a cross-flow from top to bottom is superimposed. In such a case, all streamlines crossing the line of symmetry [shown as a dotted line in Fig. 1(c)] must do so from top to bottom. This implies that the two stagnation points A and C are displaced. It can be seen from Fig. 1(b) that streamlines moving from top to bottom lie *below* A and *above* C. Therefore, in order for these streamlines to cross the line of symmetry, A must be displaced upwards and C downwards. As a result of these displacements, the streamline CA is broken, since otherwise it would cross the line of symmetry from bottom to top. Instead, the streamline from C must stay below the symmetry line and go around eddy E towards stagnation point D. The condition of incompressibility (implying that the streamlines around the eddy center E are closed) ensures that it must reach D exactly. Similarly, consideration of the flow around F shows that the streamline moving upwards from point A is a homoclinic orbit, lying entirely above the symmetry line, missing points B and C and returning to A. Thus, the effect of the small transverse perturbation is that the symmetric topology of Fig. 1(b) is broken, and replaced by that of Fig. 1(c).

For the second argument, we consider a symmetric transition from flow 1(a) to flow 1(b) as a parameter (such as the mean roller speed) is varied. In this case, the five stationary points are created at the same place and at the same value of the parameter. In contrast, for the asymmetric transition from flow 1(a) to flow 1(c), two separate transitions occur; one forming the attached eddy E, the other forming the detached eddy F. Let us consider the fluid velocity along the meniscus, v_m, as a function of the curvilinear coordinate along the meniscus, s. When the flow is recirculating this function has three zeros, corresponding to the three stagnation points on the meniscus. Only one of these points survives when there is no recirculation. Taking s to be zero at this point, and starting from the assumption that, close to the transition, the three zeros are at least close to each other, we examine the Taylor expansion of $v_m(s)$. Clearly, in order to have three zeros we need to include third order terms. Since $v_m(0)=0$, we may write

$$v_m(s)=s(\alpha+\beta s+\gamma s^2+\cdots). \tag{1}$$

The coefficients α, β, and γ each depend on the parameter (e.g., mean roller speed) controlling the flow structure. The transition to recirculation corresponds to a change of sign of $\beta^2-4\alpha\gamma$.

If the flow is exactly symmetric, then v_m is antisymmetric in s and β is thus zero. The transition then corresponds to a change of sign of α and the extra zeros appear at $s=0$. However, if the flow is asymmetric then there is no reason why β should be zero. In this case the birth of the extra zeros, with the associated eddy E, will in general occur away from $s=0$. This transition has the following local stream function representation as parameter λ passes through zero:

$$\psi=-\lambda y+x^2y+y^3, \tag{2}$$

where $y=0$ represents the meniscus locally. This transition creates only the attached eddy E. A second transition is required for the detached eddy to appear; it is of the type

$$\psi=-\lambda' y'+x'^2+x'^2y'+y'^3. \tag{3}$$

The notation x', y', and λ' emphasizes that the transition occurs at a different place and orientation, and for a different value of the parameter, than the one on the meniscus.

Depending on whether $\lambda'=0$ corresponds to a negative or a positive value of λ, there will be a range of the parameter for which there is either an internal saddle point with associated eddy but only one stagnation point on the meniscus, or an eddy attached to the meniscus but no internal eddy. These two arguments provide the theoretical basis for claiming that the recirculating flow topology seen in practice will either be that of Fig. 1(c) or of its reflection (snake going from bottom to top), depending on the source of asymmetry. The joint eddy topology will only be observed as a transitional case when the sources of asymmetry are either absent or exactly cancel each other.

In order to verify experimentally the preceding theoretical arguments, we have used the same setup as for previous studies of the meniscus [10]. It consists of two steel cylinders of radii $R_1=67.5\pm0.02$ mm and $R_2=27.5\pm0.02$ mm, respectively, with their axes located in a plane inclined at 45° to the horizontal. The width h_0 of the gap separating the cylinders can be selected to within 0.03 mm, while the accuracy on each of the (independent) tangential velocities U_1 and U_2 is ±0.2 mm/s. The subscripts 1 and 2 stand for the upper and lower roll, respectively. The lower cylinder is immersed at a depth of 10 mm in a container filled with the fluid Rhodorsil 47V500 silicone oil (Rhône-Poulenc), with dynamic viscosity $\mu=0.54$ Pa s, surface tension $\sigma=0.0209$ N/m, and density $\rho=970$ kg/m^3. For this demonstrative case, only one experiment is discussed, with $h_0=0.64$ mm, $U_1=U_2=5.4$ mm/s. Under these conditions, the corresponding dimensionless parameter, the capillary number $\mathrm{Ca}_i=\mu U_i/\sigma$, is the same for both cylinders, $\mathrm{Ca}_1=\mathrm{Ca}_2=0.14\pm0.005$. The only apparent sources of asymmetry are thus gravity and unequal roll radii. In order to implement the PIDV technique, the fluid is seeded with Iriodin 111 particles (Merck), of approximate diameter 5 μm, at a dilution of 0.8 g/dm^3. A very thin (0.1 mm) argon ion laser sheet illuminates a plane perpendicular to the cylinder axes, 40 mm from the left edge of the setup. A prism is put at that end, in contact with the fluid, acting as a window to enable a microscope to film the particles illuminated within the laser sheet. The field of vision of the IEC 800 CCD camera (i2s) is a 2.51×2.85 mm^2 box, yielding a spatial resolution of 4.9×5.5 μm^2. This window includes the meniscus region, the recirculating areas, and part of the cylinder walls (see Fig. 2). The calibration technique is the same as in previous works [10], with the exception that the optical path between the prism and the calibrating part is filled with the fluid to cancel refractive index effects. The resulting accuracy is equal to 15 μm for relative measurements (two points in the fluid) and 0.1 mm

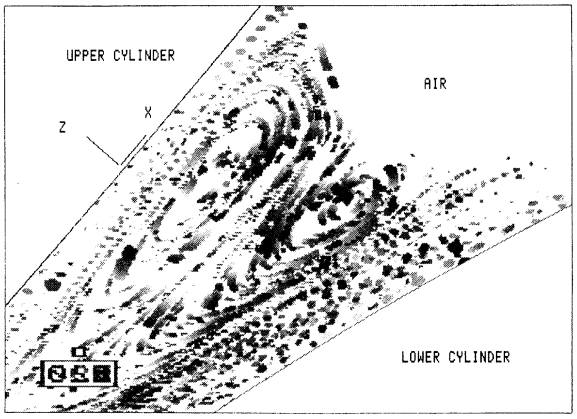

FIG. 2. Experimental particle tracking: superposition of 16 successive images. Progressive time coding in darkening gray shades: t_0 (= 0 s) light gray; t_{15} (= 0.6 s) black. The calibrated X and Z segments represent 0.25 mm.

for absolute measurements (a point in the fluid vs cylinder walls), but could be larger due to optical edge effects at the prism [9]. The flow is filmed at video rate (20 Hz) with 10 ms exposure time. First, a qualitative diagnostic of the flow can be performed by superimposing several pictures of the flow at constant time intervals. Figure 2 displays such a series of 16 successive snapshots of the flow, at intervals of 40 ms. This "particle tracking" technique clearly displays the flow topology, with a snake swirling around two disjoint eddies, only one of them attached to the interface. The two dimensionality of the flow is guaranteed by the fact that particles remain visible in the laser sheet throughout their passage in the field of vision. The particles follow the streamlines well, closing trajectories over several turnover times inside eddies. To obtain a quantitative diagnostic of the flow, PIDV is applied to two successive video images, separated by 40 ms. A cross-correlation scheme [12] is applied to the images, providing the displacement vectors on a grid of 800

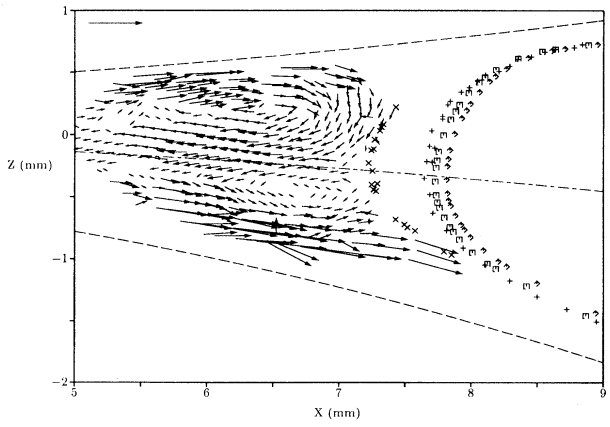

FIG. 3. Experimental 2D velocity vector plot at $h_0=0.64$ mm, $Ca_1=Ca_2=0.14$. The scaling vector in the upper left corner is 2 mm/s long. Meniscus shapes: PIV (crosses); laser fluorescence (pluses); numerical simulation, $Q/Uh_0=0.65$ (squares), $Q/Uh_0=0.7$ (diamonds).

points. The resulting velocity vectors are determined to within an accuracy of 3%, with an upper velocity limit of 2 mm/s. This is sufficient to resolve the velocity field in the eddy regions, but not closer to the cylinder walls, where $U=5.4$ mm/s. The measured velocity field is displayed in Fig. 3. The origin is located in the middle of the nip, and the Z axis joins the centers of the cylinders. The recirculating features are well apparent, with the snake in between. The meniscus position is determined midway between each particle and its reflection in the interface. This is a potential source of inaccuracy, as the interface acts as a mirror of as yet unknown shape. Estimation of the flow rate from the measured velocity profile yields $Q/Uh_0=0.7\pm0.07$ [13], with U as the mean velocity $(U_1+U_2)/2$. In order to confirm these measurements, a technique based on laser fluorescence [10] is used to obtain the interface profile, and the flow rate by film thicknesses. The result of this technique is displayed in Fig. 3. The difference in streamwise position of the interface ($\Delta X\approx0.4$ mm) exceeds the estimated absolute uncertainties. Two reasons can be put forward: uncertainty on the capillary numbers, which can have a strong influence on the total flow rate at those low velocities, and uncertainty of the exact location of the interface between each particle and its reflection. $Q/Uh_0=0.69\pm0.05$ confirms measurements inside the flow. It should be noted that, due to the low capillary number, the value of Q/Uh_0 is lower than the usual value of $Q/Uh_0=4/3$ encountered in fully flooded roll coating. However, this value is high enough to avoid reverse flow in the nip region (the case known as *meniscus coating* [7]), thereby guaranteeing that the observed features are genuine to film splitting. We have observed the same topology for other conditions where $U_1\neq U_2$, keeping the gap width and the mean roller speed constant.

In order to compare the preceding results with numerical simulations of the flow, we have used the spectral element fluid analysis program NEKTON Version 2.85 [14]. The two-dimensional (2D) computational domain reproduces the experimental setup described previously from the nip downstream to the films at angular positions of 12° and 31° from the nip for the upper and lower cylinders, respectively. The fluid properties duplicate the experiment. Advection terms are neglected since the Reynolds number is low (Re $=\rho U_1 h_0/\mu=0.006$), and NEKTON is used to solve a steady Stokes flow problem, taking gravity into account. The boundary conditions are the following: Cylinder walls moving at 5.4 mm/s, free surface conditions along the meniscus, and across each film outlet $T_n=0$, and $u_t=0$, where T_n refers to the normal traction and u_t to the tangential velocity, in the local coordinate system. Cases are run for two inlet parabolic flows, at flow rates $Q/Uh_0=0.7$ and 0.65, to account for experimental uncertainty. The initial shape of the free surface is estimated from the experimental results, then it is computed up to convergence (normalized change in mesh coordinates lower than 10^{-4}) using a remeshing algorithm. With $Ca=0.14$, the viscous forces are smaller than the surface tension effects so that a surface tension dominant algorithm is used. The mesh consists of 44 spectral elements, and Legendre polynomials of fifth order are used as trial functions in each macroelement. The resulting stream function pattern for $Q/Uh_0=0.65$ is displayed near the interface in Fig. 4. The calculated meniscus shapes for both cases are superimposed

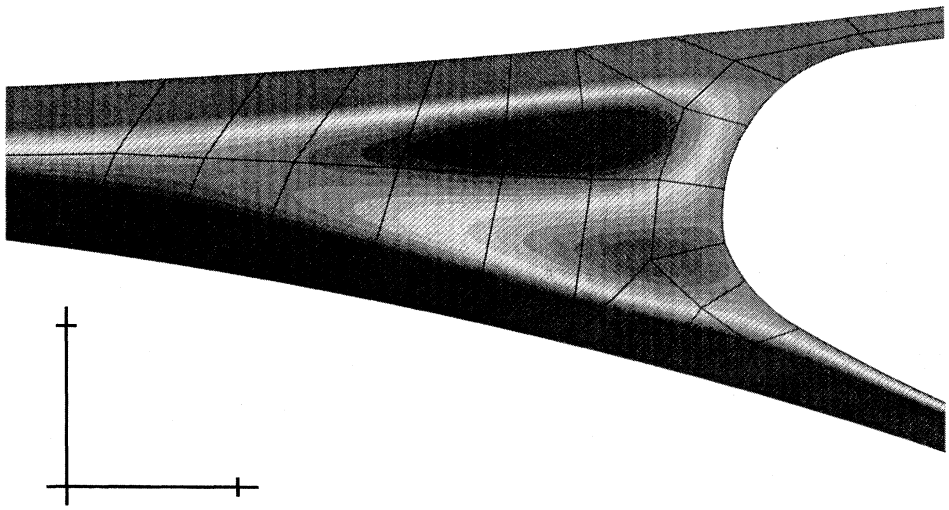

FIG. 4. Numerical simulation at $h_0=0.64$ mm, $Ca_1=Ca_2=0.14$, $Q/Uh_0=0.65$. Mesh structure and stream function ψ. $\psi=0$ is located at midgap in the nip. The stream function pattern within the interval $\psi/Uh_0 \in [-870,145]$ is displayed. The scale in the lower left corner represents 1 mm.

in Fig. 3. The difference of 0.05 in the total flow rates causes a streamwise displacement of 0.12 mm, showing the sensitivity of meniscus position versus flow rate. The numerical curve at $Q/Uh_0=0.65$ is seen to be in very good agreement with the fluorescence experiment, calling for improved accuracy in PIDV calibration. These results confirm theoretical arguments about the asymmetric flow topology.

In conclusion, theoretical, experimental, and numerical results show that stable asymmetric film-splitting flows with recirculation are generally of the disjoint eddy type. Further work will have to address the question of which bifurcation scenarios are followed between different topologies. In particular, it will be interesting to clarify in which order the internal and attached eddies appear as parameters are varied, and to see how several asymmetry sources can cancel each other to display joint eddy topology.

[1] S. Michalland, M. Rabaud, and Y. Couder, Europhys. Lett. **22**, 17 (1993); L. Pan and J.R. de Bruyn, Phys. Rev. Lett. **70**, 1791 (1993); M. Rabaud, S. Michalland, and Y. Couder, *ibid.* **64**, 184 (1990).

[2] G.C. Carter and M.D. Savage, Math. Eng. Ind. **1** (1), 83 (1987); D.J. Coyle, C.W. Macosko, and L.E. Scriven, J. Fluid Mech. **216**, 437 (1990); M.D. Savage, AIChE J. **30** (6), 999 (1984); G.I. Taylor, J. Fluid Mech. **16**, 595 (1963).

[3] H.K. Moffatt, J. Fluid Mech. **18**, 1 (1964); J.-T. Jeong and H.K. Moffatt, *ibid.* **241**, 1 (1992).

[4] E. Pitts and J. Greiller, J. Fluid Mech. **11**, 33 (1961); M.D. Savage, *ibid.* **117**, 443 (1982).

[5] D.J. Coyle, C.W. Macosko, and L.E. Scriven, J. Fluid Mech. **171**, 183 (1986).

[6] H.M. Thompson, Ph.D. Thesis, University of Leeds, 1992; M.E. Gurfinkel Castillo and A.T. Patera (unpublished).

[7] B. Malone, Ph.D. Thesis, University of Leeds, 1992 (unpublished).

[8] G.B. Schneider, Trans. Soc. Rheol. **VI**, 209 (1962); M. Decré, Ph. D. thesis, Université Paris VI, 1994 (unpublished).

[9] P.M. Schweizer, J. Fluid Mech. **193**, 285 (1988).

[10] M. Decré and J.M. Buchlin, Exp. Fluids **16** (5), 339 (1994); M. Decré, E. Gailly, and J.-M. Buchlin, Phys. Fluids **7** (3), 458 (1995).

[11] R.J. Adrian, Annu. Rev. Fluid Mech. **23**, 261 (1991).

[12] G. De Potter, von Karman Institute, Rhode-Saint-Genèse Report No. 1992-01, 1992 (unpublished).

[13] The velocity field is linearly interpolated from the last valid point to the wall value of 5.4 mm/s, then integrated with a Newton scheme. Performing this across the channel width at several streamwise positions and taking the linear interpolation into account provides the uncertainty of 0.07.

[14] NEKTON is a registered trademark of Nektonics Incorporated and the Massachusetts Institute of Technology and is distributed and supported by Fluent Inc.

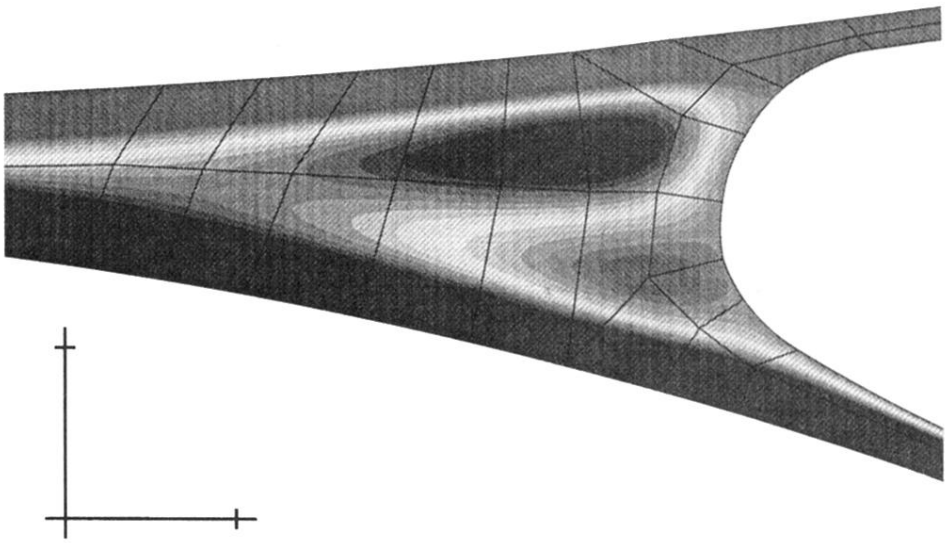

FIG. 4. Numerical simulation at $h_0=0.64$ mm, $Ca_1=Ca_2=0.14$, $Q/Uh_0=0.65$. Mesh structure and stream function ψ. $\psi=0$ is located at midgap in the nip. The stream function pattern within the interval $\psi/Uh_0\in[-870,145]$ is displayed. The scale in the lower left corner represents 1 mm.